

A Particle Dynamic Model of Red Blood Cell Aggregation Kinetics

MARIANNE FENECH,^{1,4} DAMIEN GARCIA,¹ HERBERT J. MEISELMAN,² and GUY CLOUTIER^{1,3,5}

¹Laboratory of Biorheology and Medical Ultrasonics, University of Montreal Hospital Research Center (CRCHUM), Montréal, QC, Canada; ²Department of Physiology and Biophysics, Keck School of Medicine, University of Southern California, Los Angeles, USA; ³Department of Radiology, Radio-Oncology and Nuclear Medicine, and Institute of Biomedical Engineering, University of Montreal, Montréal, QC, Canada; ⁴Present Address: Department of Mechanical Engineering, University of Ottawa, Ottawa, ON, Canada; and ⁵Research Center, University of Montreal Hospital (CRCHUM), Pavillon J.A. De Séve (Room Y-1619), 2099 Alexandre de Séve, Montréal, QC H2L 2W5, Canada

(Received 23 September 2008; accepted 31 July 2009; published online 11 August 2009)

Abstract—To elucidate the relationship between microscopic red blood cell (RBC) interactions and macroscopic rheological behavior, we propose a two-dimensional particle model capable of mimicking the main characteristics of RBC aggregation kinetics. The mechanical model of RBCs sheared in Couette flow is based on Newton law. We assumed a hydrodynamic force to move particles, a force to describe aggregation and an elasticity force. The role of molecular mass and concentration of neutral polymers on aggregation [Neu, B., and H. J. Meiselman. *Biophys. J.* 83:2482–2490, 2002] could be mimicked. Specifically, it was shown that for any shear rate (SR), the mean aggregate size (MAS) grew with time until it reached a constant value, which is consistent with *in vitro* experiments. It was also demonstrated that we could mimic the modal relationship between MAS and SR and the occurrence of maximum aggregation at about 0.1 s^{-1} . As anticipated, simulations indicated that an increase in aggregation force augmented MAS. Further, augmentation of the depletion layer thickness influenced MAS only for SR close to zero, which is a new finding. To conclude, our contribution reveals that the aggregation force intensity and SR influence the steady state MAS, and that the depletion and layer thickness affect the aggregation speed.

Keywords—Erythrocyte aggregation, Modeling, Mean aggregate size, Blood flow rheology, Couette flow, Depletion force, Erythrocyte, Shear rate.

NOMENCLATURE

A, B, D, δ_0	Aggregation force constitutive parameters
d_{ij}	Distance between centers of mass of RBCs i and j
\mathbf{e}_i^0	Normalized vector of the driving velocity for each RBC i

\mathbf{f}_{ij}^a	Aggregation force from RBCs j to i
\mathbf{f}_{ij}^e	Elasticity force from RBCs j to i
\mathbf{f}_i^h	Estimated hydrodynamic force
H	Hematocrit
k	Elasticity coefficient
MAS	Mean aggregate size
m_i	Mass of RBC i
\mathbf{n}_{ij}	Normalized vector pointing from RBCs j to i
R	Radius of RBCs
RBC	Red blood cell
ROI	Region of interest
δ	Membrane cell-to-cell distance
r_i	Position of the RBC i center of mass
SR	Shear rate
t	Time
\mathbf{v}_i	RBC i velocity vector
v_i^0	RBC i driving speed
Φ	Interaction energy potential

INTRODUCTION

Under normal physiological conditions, for athletic mammal species, red blood cells (RBCs) form reversible aggregates in slow flow that usually take the form of rouleaux or complex three-dimensional structures. When the flow rate is increased, shearing forces disaggregate rouleaux, and RBCs return to their individual state. Erythrocyte aggregation is an important physiological phenomenon almost totally responsible for the non-Newtonian flow behavior of blood, and the effects of the molecular mass and concentration of neutral polymers [e.g., dextran, poly(ethylene glycol)] are of basic science and clinical interest.^{2,22,23,29} However, the specific mechanisms involved in RBC aggregation have not yet been fully elucidated, and two models have been proposed: (a) bridging of cells by

Address correspondence to Guy Cloutier, Research Center, University of Montreal Hospital (CRCHUM), Pavillon J.A. De Séve (Room Y-1619), 2099 Alexandre de Séve, Montréal, QC H2L 2W5, Canada. Electronic mail: guy.cloutier@umontreal.ca

cross-linking macromolecules¹¹; and (b) attractive forces due to osmotic gradients generated by the depletion of macromolecules in intercellular spaces.^{4,24,25} The depletion model was considered for the present study. In the depletion theory, cell–cell interactions are complex processes which involve, as a first approximation, a balance between depletion attractive forces and electrostatic repulsive forces. The analytical approach describing the interaction energy between RBCs in polymer solutions, proposed by Neu and Meiselman,²⁴ was specifically used in this study to model aggregation.

Numerical methods manageable to mimic a wide range of physiological flow conditions are rare. Models considering particle interactions are usually limited to the study of a small number of cells. Recently, two or three-dimensional intricate numerical models were proposed.^{3,6,15,26,28,34} These simulations were able to reveal complex behaviors of RBCs in microvascular flow, such as cell deformation, clustering, rolling or migration. Although very informative, the abovementioned numerical models are relatively arduous to be implemented and, above all, their computation time is intensive so that it could be strenuous to investigate a large number of RBCs over a wide range of pathophysiological conditions. Also, besides Liu and coworkers,^{20,21} the depletion theory was not explicitly considered in these models. These last authors used the aggregation force from the depletion model in a mechanical flow dynamic study: their innovative method consisted of coupling solutions of the Navier–Stokes equation and protein molecular dynamics, and examined the deformation and aggregation of three-dimensional biconcave RBCs. Other earlier theoretical approaches proposed for describing aggregation with a larger number of RBCs were based on modeling the kinetics of a colloidal suspension,^{9,19} but the method had limited validity for describing the details of aggregated structures. Our group has designed a model stemming from elementary displacements of RBCs,¹⁶ but aggregation forces were not specifically considered.

This study was undertaken to evaluate the impact of forces from the depletion model on RBC aggregation and rheological properties from a microscopic, mechanical point of view in order to clarify the relationship between microscopic RBC interactions and macroscopic rheological behavior. The goals of the current study were: (a) to develop and assess a model of aggregation kinetic based on the mechanical interaction of RBCs; and (b) to investigate the influence of aggregation forces.

In overview, our model was inspired by the work of Helbing *et al.*¹⁷ who proposed a model of traffic dynamic of many particle systems, to simulate for example in their *Nature* paper, the dynamic features

of humans trying to escape from a closed environment.¹⁷ This mechanical strategy allows point-mechanics computation with the aims to work with a large number of cells thus making the analysis more manageable over a large range of physiological conditions.

First, we describe the mechanical model, focusing on RBC interacting forces. We then report results from calculations representing the effects of shear rate (SR), and the production of aggregation forces for cells in polymer solutions. Both the effects of molecular mass and concentration of neutral polymers are discussed. Then, to assess the model, the results are compared with existing experimental data; the model's limitations are summarized and potential applications are discussed.

METHODS

Blood and RBC Particle Model

Blood was considered as a collection of particles of radius R interacting between each other, and the flow field was modeled as a Couette flow since this configuration is characterized by a constant shear rate and hence by well-defined fluid mechanics within the region of interest.

According to the second Newton's law, the acceleration of a particle i over time t is given by:

$$m_i \frac{d\mathbf{v}_i}{dt} = \sum_{i \neq j} \mathbf{f}_{ij} + \mathbf{f}_i^h, \quad (1)$$

where m_i is the mass of particle i ($m_i = m$), and \mathbf{v}_i is its velocity vector. The vector \mathbf{f}_{ij} represents the force of particle j acting on particle i and \mathbf{f}_i^h is the estimated hydrodynamic force. Using an iterative process, velocities and positions of all particles at time $t + dt$ were deduced from the acceleration at each instant t according to Eq. (1).

Elastic Force

We investigated two interaction forces to describe RBC aggregation, namely an aggregation force \mathbf{f}_{ij}^a and an elastic force \mathbf{f}_{ij}^e . The total force imposed by particle j on particle i was thus $\mathbf{f}_{ij} = \mathbf{f}_{ij}^a + \mathbf{f}_{ij}^e$. The elastic force was based on a granular interaction model¹⁴ and was given by:

$$\begin{aligned} \mathbf{f}_{ij}^e &= k(2R - d_{ij})^{3/2} \mathbf{n}_{ij} \quad \text{if } d_{ij} < 2R \\ &= 0 \quad \text{otherwise} \end{aligned} \quad (2)$$

where d_{ij} represents the distance between the respective centers of mass of RBCs i and j , and \mathbf{n}_{ij} is the

normalized vector pointing from RBCs j to i . Equation (2) indicates that this force tends to repel RBCs when the distance between their centers of mass is smaller than the cell diameter $2R$. Because its amplitude is not infinite when $d_{ij} < 2R$, RBCs are not considered rigid and may be compressed by a factor modulated by the elastic modulus k . However, in this study we did not investigate the impact of RBC rigidity on flow; the elastic modulus k was fixed at 3×10^{-6} N/m based upon reported values.^{13,33}

Aggregation Force

We considered the depletion theory developed by Neu and Meiselman,²⁴ but the complex equations developed by them could not be easily adapted to our model. We therefore adopted the potential approach, including attracting depletion and repulsive electrostatic interaction energies, as previously examined by Liu and coworkers.^{20,21} This approach can be expressed as a function of only three independent parameters:

$$\Phi_{ij} = D \left(e^{2B(\delta_0 - \delta_{ij})} - 2e^{B(\delta_0 - \delta_{ij})} \right), \quad (3)$$

where Φ_{ij} is called the Morse potential and represents the interaction energy between two particles. This potential between RBCs i and j depends upon a coefficient of surface energy D , the membrane cell–cell distance $\delta_{ij} = (d_{ij} - 2R)$, the membrane cell–cell distance δ_0 for which the aggregation force is zero, and a scaling factor B ; the factor B is inversely related to the depletion layer thickness. The aggregation force resulting from the Morse potential and acting on RBC i can then be expressed as²¹:

$$\mathbf{f}_{ij}^a = -\frac{\partial \Phi_{ij}}{\partial \delta_{ij}} A = 2DAB \left(e^{2B(\delta_0 - \delta_{ij})} - e^{B(\delta_0 - \delta_{ij})} \right) \mathbf{n}_{ij} \quad (4)$$

where A is the area of RBC surface in face to face apposition with another RBC. The Morse potential and the resulting aggregation force as a function of separation are shown in Fig. 1.

Values of parameters B , δ_0 and D in Eq. (3) were adapted from the interaction energy profiles depicted in Fig. 3 of Neu and Meiselman²⁴ in order to capture force variations close to the cell with a reasonable time-step while respecting the ratio between physiological aggregation and hydrodynamic forces. Indeed, parameters extracted from Neu and Meiselman's study resulted in intensive computations since very small time-steps were necessary to capture force interaction variations close to the cell. In consequence, to maintain a consistent model, an adimensional analysis suggested the use of a constant drag force for all calculations.

Aggregation could be increased either by augmenting D or by decreasing B . The former corresponds to an increment of force amplitude that may be observed when raising the concentration of polymers in the suspending solution. The latter is related to an increase in depletion layer thickness (i.e., interaction distance) while energy intensity remains unchanged; this phenomenon may be seen with polymers of increasing molecular size having the same suspending medium concentration.²⁴ Initially, aggregation was modulated from a low to a high level using a range of energy (DA) between 10^{-26} and 5×10^{-23} J. The effect of the depletion layer thickness was studied by changing B between $0.2 \mu\text{m}^{-1}$ and 0.2nm^{-1} while the product DAB was maintained constant. For clarity, the three forces studied were termed Agg^- , Agg^+ and $\text{Agg}^{+\frac{1}{2}B}$, corresponding respectively to low aggregation, high aggregation, and, in the last case, to a thicker depletion layer thickness than with force Agg^+ . The corresponding values of B , DA and δ_0 for these specific forces are summarized in Table 1 and the aggregation forces resulting from these three conditions are compared in Fig. 1. It is important to note that the coefficients B^+ and DA^+ for force Agg^+ (Table 1) are

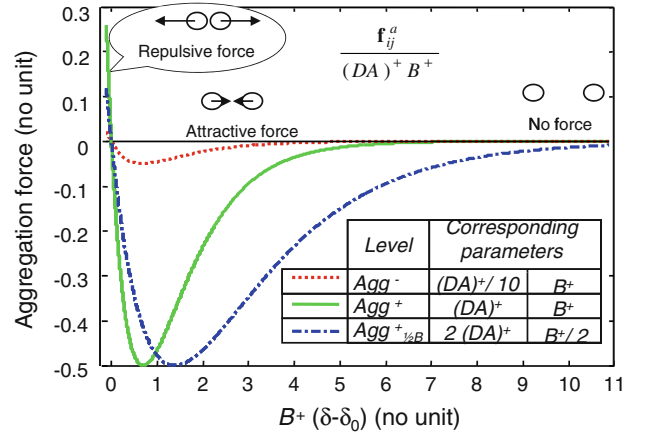


FIGURE 1. Influence of parameters B and DA on the non-dimensional aggregation force $\frac{f_{ij}^a}{(DA)^+ B^+}$, where DA is the coefficient of energy and B is a scaling factor. Increasing DA leads to a stronger adhesion force, corresponding to escalating concentrations of polymer in the suspending medium. On the other hand, decreasing B and increasing DA proportionally raises the depletion layer thickness corresponding to augmenting molecular masses of the dissolved polymer.

TABLE 1. Constitutive parameters for three selected aggregation forces.

	Agg^-	Agg^+	$\text{Agg}^{+\frac{1}{2}B}$
δ_0 : Zero-force length (nm)	11	11	11
DA : Energy (J)	10^{-25}	10^{-24}	2×10^{-24}
B : Scaling factor (m^{-1})	10^7	10^7	5×10^6

used hereafter as reference values for normalizing results.

Estimated Hydrodynamic Force

We assumed a spherical solid particle, isolated, with a very small Reynolds number (<1), and a very small Stokes number (<0.005). Under these conditions, the estimated hydrodynamic force induced by the Stokes drag on a sphere is given by Eq. (5):

$$\mathbf{f}_i^h = 6\pi\mu R(v_i^0 \mathbf{e}_i^0 - \mathbf{v}_i) \quad (5)$$

where μ is the dynamic viscosity of the fluid, R is the radius of the particle, $v_i^0 \mathbf{e}_i^0$ denotes the velocity of the fluid in the absence of particles, which drives the particle i to flow along the direction \mathbf{e}_i^0 at a speed v_i^0 , and \mathbf{v}_i is the current particle velocity. Note that the velocity of the fluid when no particle is present is defined, for a Couette flow system, as $v_i^0 \mathbf{e}_i^0 = \text{SR } y\mathbf{x}$, where y is the coordinate defined in Fig. 2 and \mathbf{x} is the flow direction.

Simulation Approach

RBCs were modeled as spheres (moving in a plane) of radius $R = 2.7 \mu\text{m}$ to match a RBC volume of $87 \mu\text{m}^3$ as described earlier,¹⁶ and their mass m was 9.8×10^{-14} kg. The particles were initially positioned randomly without overlap in a bi-dimensional space of $250 \times 250 \mu\text{m}^2$ at a hematocrit (H) of 40%, giving a total of 1091 particles in the region of interest (ROI) of the Couette flow system.

Cyclic boundary conditions were imposed in the flow direction: each particle leaving the ROI was positioned at the ROI's entrance at the same y -coordinate with the same acceleration, velocity, and force vectors. Also a RBC located in the ROI's entrance was considered to be adjacent to a RBC in the ROI's exit

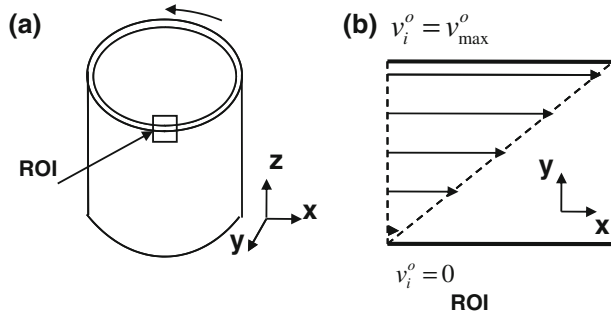


FIGURE 2. (a) The 2 coaxial cylinders composing the Couette flow system. The Region of Interest (ROI) is located in the small gap between the two cylinders. The x axis refers to the direction of flow parallel to the cylinders, and the y axis refers to the radial direction between the cylinders. (b) Magnification of the ROI and illustration of the driving velocity profile v_i^0 in the Couette flow system that results in a constant SR.

and consequently could be considered to be in the same aggregate.

The time step utilized at each iteration was selected to obtain maximal displacements of $0.05 \mu\text{m}$ for all RBCs; this method offered a reasonable compromise between the stability of the numerical results and the time for computation. Forces acting on a given RBC were calculated by considering only neighboring RBCs located within a domain of influence. The “influence radius” depended upon scaling factor B of the aggregation force expression and was defined as $20/B + 2R$. Twelve different SRs, ranging from 0.001 to 20 s^{-1} , were simulated and the velocity of RBC i was calculated from its y -position and SR, as mentioned above. Aggregation kinetics were described by the mean aggregate size (MAS) as a function of time. Using a finite difference scheme, velocities and positions of particles at time $t + dt$ were deduced from the acceleration at instant t . Single RBCs were not considered as aggregates of size 1 so that they did not influence the number of aggregates or MAS. Two RBCs were aggregated if the distance between their centers was within 2% of their diameter. The code was implemented in C++ to obtain RBC positions, and post-processing was done with Matlab (version 7.0.1., The MathWorks, Natick, MA, USA).

RESULTS

This section considers in order: (1) the kinetics of aggregation; (2) the effects of SR; (3) the effects of the aggregation force intensity; (4) the effects of varying the depletion layer; and (5) the effects of imposing pulsatile SRs. For the sake of clarity, a logarithmic scale is used for MAS and SR in Figs. 4–8.

Kinetics of Aggregation

Figure 3 (top) presents an example of kinetics for the aggregation force Agg^+ and a $\text{SR} = 0.1 \text{ s}^{-1}$. The percentage of aggregated RBCs and MAS increased with time and reached a plateau, in agreement with the reduction in the number of aggregates over time. As expected, aggregation is a time-dependent phenomenon.^{10,11} The bottom panels show the simulated spatial organization of RBCs for three time increments.

Effects of SR

The time course of MAS for SRs varying between 10^{-3} and 10 s^{-1} for the simulated conditions corresponding to Agg^+ are illustrated in Fig. 4. To match experimental results, no simulations were allowed to

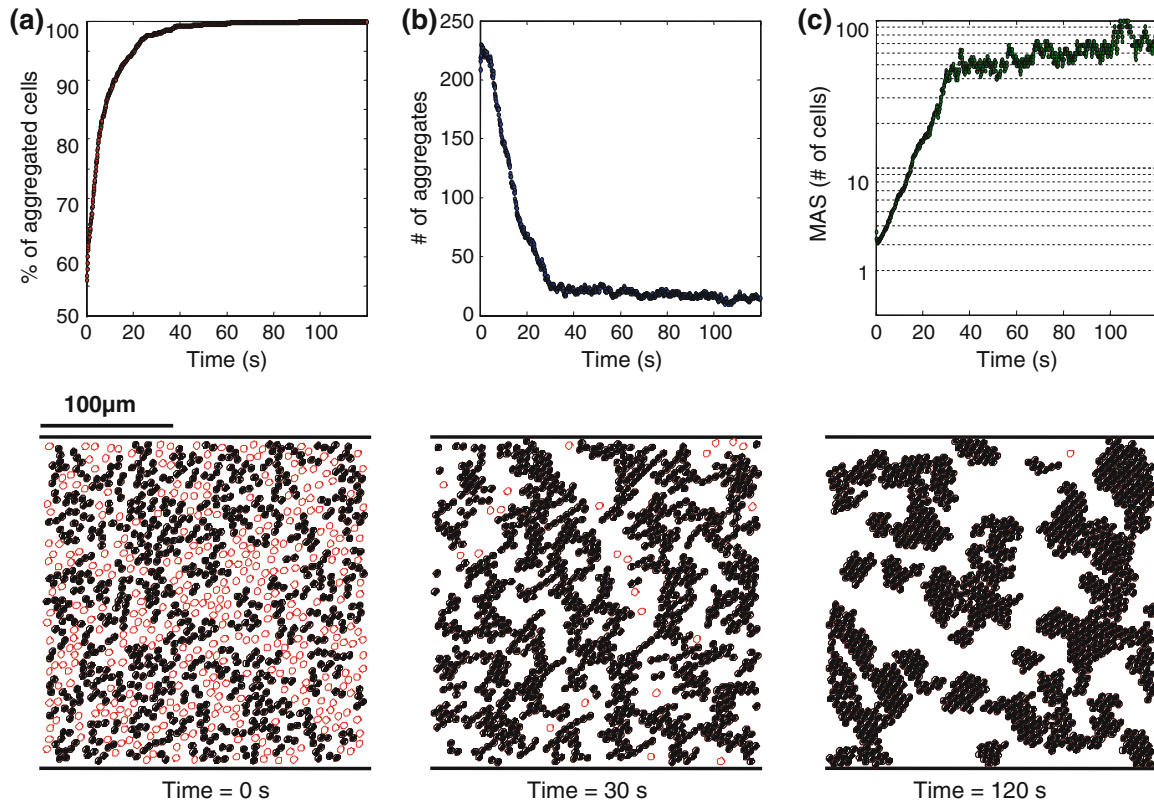


FIGURE 3. RBC aggregation kinetics as a function of time for $SR = 0.1 \text{ s}^{-1}$ and $Agg^+ (DA = 10^{-24} \text{ J}, B = 10^7 \text{ m}^{-1})$. *Top panels:* (a) percentage of aggregated cells; (b) number of aggregates; (c) MAS as a function of time. *Bottom panels:* Corresponding simulation results for three different times. Empty and filled circles represent non-aggregated and aggregated cells, respectively.

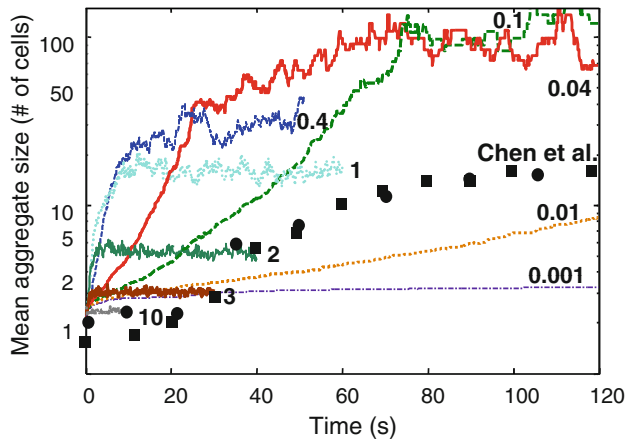


FIGURE 4. Temporal evolution of MAS for different SRs. The simulations shown are for Agg^+ conditions (see Table 1). Numbers beside each line are SR in s^{-1} . Black squares and circles are two experiments on median aggregate sizes for fresh human blood at rest for a hematocrit of 10%. “Spontaneous aggregation” (SR not known) was induced by the addition of 0.5% dextran 500 kDa to blood (data reproduced from Chen *et al.*¹⁰).

run beyond 120 s. The largest aggregates at the plateau region were observed for SRs between 0.04 and 0.1 s^{-1} . Note that the dependency of aggregate size at

the plateau region on SR reflects the non-Newtonian viscosity behavior of blood (assuming that viscosity increases with MAS). For SRs higher than 1 s^{-1} , the convergence time to reach equilibrium MAS was smaller than 15 s, but for SRs lower than 0.1 s^{-1} the aggregation plateau was still not reached at 120 s.

Figure 5 presents MAS, at 120 s or earlier if steady state was reached, vs. SR for three aggregation forces (i.e., Agg^- , Agg^+ , $Agg_{\frac{1}{2}B}^+$). The MAS increased to a maximum between 0.04 and 0.1 s^{-1} , then declined to a minimum close to a value of 2 at higher shear rates. The kinetics of aggregation provides an explanation for the modal relationship between aggregate size and SR. For SRs smaller than 0.1 s^{-1} , aggregation is a slow process and the plateau of MAS can not be reached: consequently, the maximum size of aggregates is not completely attained. This situation parallels that of several experimental studies that can be found in the literature where analyzes were stopped at 120 s.

Note that the minimum size was reached for a SR of 5 s^{-1} for the force Agg^+ , and for a SR of 3 s^{-1} for the force Agg^- , and hence the expected result that a higher SR is needed for disaggregation if the aggregation force is higher. The simulated condition for a larger depletion layer thickness (i.e., $Agg_{\frac{1}{2}B}^+$) gave results

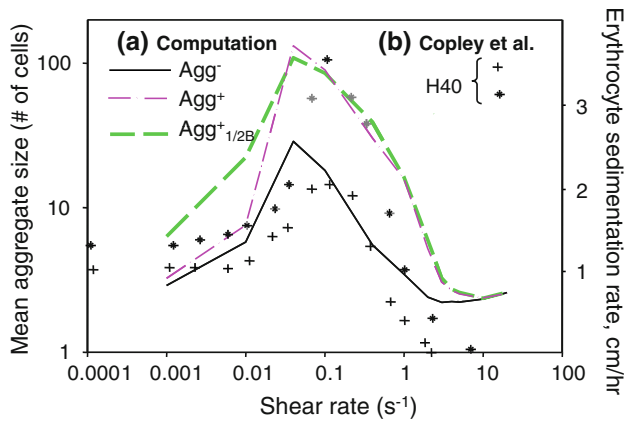


FIGURE 5. (a) Computational results of the effect of SR on MAS at either steady state or at 120 s. Three forces of aggregation were used: Agg⁻, Agg⁺, Agg^{+1/2B} (see Table 1). (b) Two experiments on the erythrocyte sedimentation rate (cm/h) for fresh human blood at 40% hematocrit (data reproduced from Copley *et al.*¹²).

similar to Agg⁺ for SRs greater than 0.4 s⁻¹, whereas for smaller SRs, MAS was larger for Agg^{+1/2B} (Fig. 5).

Effects of Varying the Aggregation Force Intensity

To focus on the effect of the force intensity due to the concentration of polymers in the solution, Fig. 6 gives examples of MAS vs. energy (*DA*) for four SRs. MAS is reported at the steady-state or at 120 s if the steady-state was not reached earlier, in agreement with an existing experimental protocol³⁰ and a theoretical study.¹⁹ As expected, MAS increased with increasing force intensity. A power law dependence (i.e., linear model on log-log coordinates) for MAS > 2 was obtained between MAS and *DA* (*p* < 0.001, Sigma-Stat, version 3.11, Systat Software, San Jose, CA, USA). The following power law relationship was obtained:

$$MAS = MAS^+ \left(\frac{DA}{(DA)^+} \right)^{0.73} \quad (6)$$

where MAS⁺ is the MAS for the given SR at force Agg⁺. These results thus reflect the balance between cell aggregation forces and the dispersing effect of SR. In Fig. 6, the intersection of the sloped dotted lines with the horizontal dashed line at MAS = 2 indicates that forces due to SR and elasticity exceed the aggregation force and hence aggregation is at a minimum; recall that MAS = 2 was the lowest possible value since we did not include single cells in the evaluation of MAS. Intersections between any vertical line and the power dependence lines are conditions where aggregate forces are in equilibrium with other forces; as an example, a vertical line at (DA)/(DA)⁺ = 1 is shown in

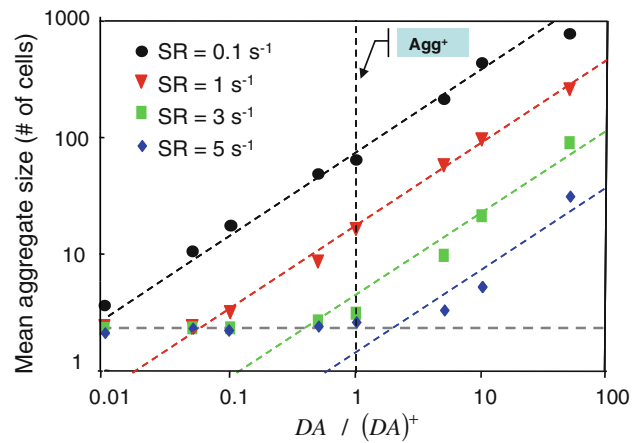


FIGURE 6. Effect of the aggregation energy (*DA*) on the MAS at steady-state or at 120 s for four levels of SR. The dashed horizontal line indicates the non-aggregated state, and the sloped dotted lines represent the power dependence between energy and MAS. The intersection of the horizontal dashed line and the sloped dotted lines indicate where aggregate forces are in equilibrium with the other forces. Seems like intersection is at MAS = 2. The Agg⁺ vertical dotted line shows the simulation at the Agg⁺ force indicated in Table 1 [i.e., *DA*/*(DA)*⁺ equals unity].

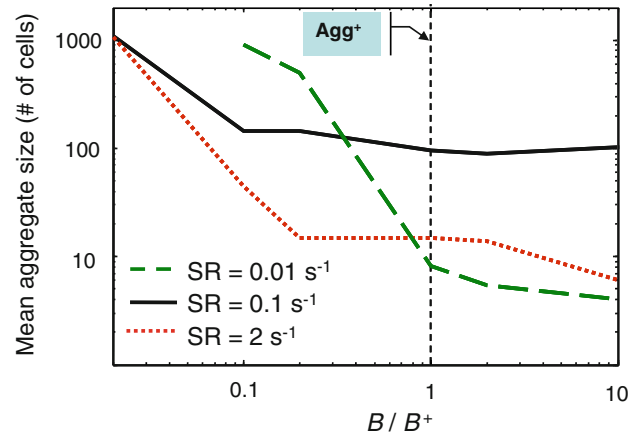


FIGURE 7. Effect of parameter *B*, which is inversely related to the depletion layer thickness, on the MAS at steady state or at 120 s. Three SRs are illustrated. The Agg⁺ vertical dotted line shows the simulation at the Agg⁺ force indicated in Table 1.

Fig. 6. As anticipated, these points of intersection are SR-dependent.

Effects of Varying the Depletion Layer

As expected, larger depletion layer thicknesses (i.e., *B* < *B*⁺) resulted in larger clusters because more RBCs were recruited (Fig. 7). However, a smaller depletion layer thickness (i.e., *B* > 0.2*B*⁺) did not markedly influence the MAS provided that MAS had reached a plateau. As shown in Fig. 8 (left), the aggregation

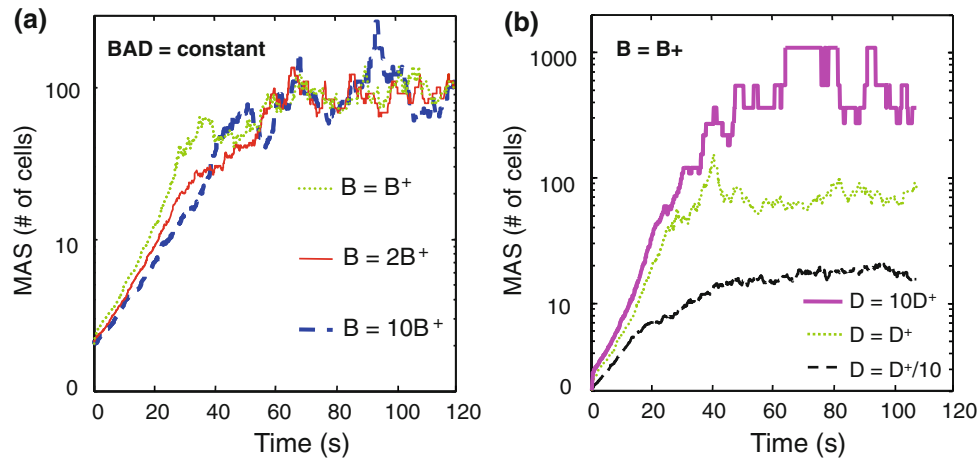


FIGURE 8. Influence of (left) B and (right) AD on aggregation kinetics. Simulations are for $SR = 0.1 \text{ s}^{-1}$. The + notation refers to the force Agg^+ indicated in Table 1.

velocity was found to be inversely related to B , whereas the magnitude of B did not affect the steady state value of MAS. Conversely, MAS values differed if, at a specific time, the aggregation velocity was unequal and the plateau had not been reached; for example in Fig. 7 for $SR = 0.01 \text{ s}^{-1}$ and in Fig. 5 if Agg^+ and $\text{Agg}_{\frac{1}{2}B}^+$ are compared for SRs less than 0.1 s^{-1} . As also noted in Fig. 8 (right), the aggregation velocity and the steady state value of MAS were proportional to D .

Effects of Imposing Pulsatile SRs

In order to underline the consequences of aggregation kinetics as an important factor leading to the rheological complexity of blood, simulations with non-constant SRs were done. First, starting from an aggregated state, SR was increased linearly for a period of time $t_0 = 23.8 \text{ s}$, then decreased linearly to reach zero at time $2t_0 = 47.6 \text{ s}$ (Fig. 9). As expected, at a given maximum SR, MAS has a different value when the SR is increasing compared to when it is decreasing. Secondly, starting from a disaggregated state, a cyclic SR was applied (Fig. 10). In this case too, at a given SR the MAS were different for increasing vs. decreasing SR even though the initial and final MAS were the same. This behavior is the signature of a hysteresis. In the light of these results, it is clear that according to our model, MAS is not only a function of SR but also depends on SR history and on the initial aggregate state.

DISCUSSION

This section is subdivided into two parts: (1) the simulation results will be compared with existing

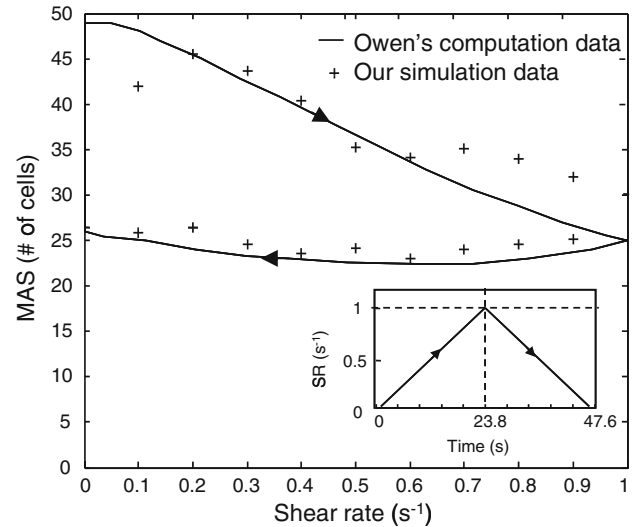


FIGURE 9. Hysteresis effect when a reversible increment of SR is applied on aggregated RBCs. The SR increases linearly to a maximum of 1 s^{-1} at $t = 23.8 \text{ s}$ before returning linearly to zero at $t = 47.6 \text{ s}$. In these simulations, $B = 10^7$ and $DA = 3 \times 10^{-26}$. Data reproduced from Owens²⁷ are illustrated on this figure.

experimental data to validate the model; and (2) the validity of the model will be discussed.

Comparison with Existing Experimental Data

We mainly chose to compare our simulation results with optical microscopy since such a method provides direct visual information regarding RBC aggregation. Conversely, methods such as viscometry, laser scattering, sedimentation, ultrasound scattering, and dielectric analyzes are indirect techniques and require

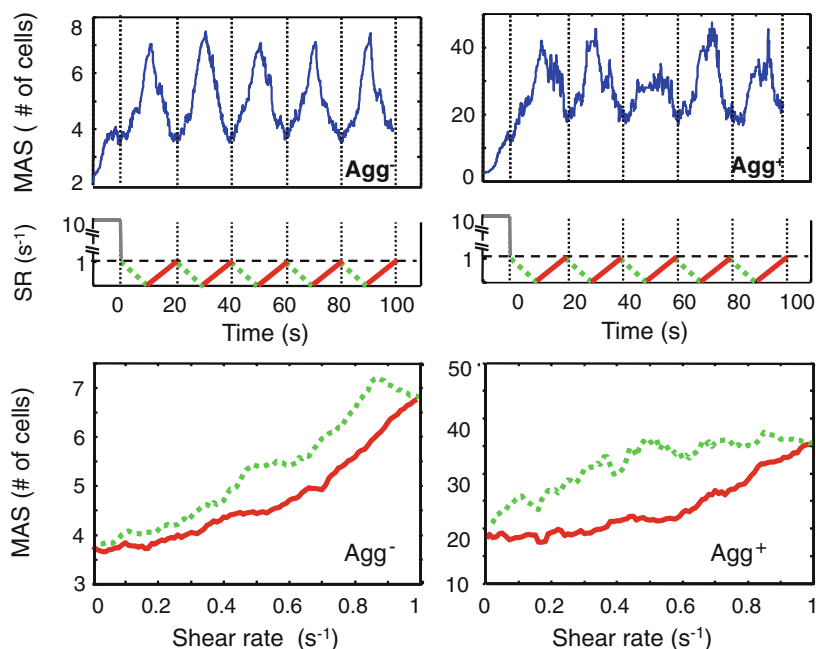


FIGURE 10. Hysteresis of MAS for an average of 5 cyclic SR applications varying between 0 and 1 s^{-1} . Forces Agg^- and Agg^+ are depicted in Table 1. Top: MAS vs. time; middle: corresponding SRs; Bottom: MAS vs. SR.

interpretation of data to obtain information on aggregation.³¹

Kinetics of Aggregation

Computed MAS–time rate results as functions of shear rate in Fig. 4 are consistent with results of Chen *et al.*,¹⁰ who studied the “spontaneous aggregation” (i.e., that the SR was not known but presumably low) of RBCs suspended in phosphate buffer solution supplemented with plasma, albumin and 500 kDa dextran. Indeed, note that in both Fig. 4, at a low shear rate, and in the work by Chen *et al.*,¹⁰ the plateau of the kinetic curves were reached at approximately 120 s after complete disaggregation and an abrupt cessation of shear.

Effects of SR

Chen *et al.*¹⁰ reported a unimodal relationship between MAS and shear stress with the occurrence of maximum aggregation at about 0.25 dyn/cm^2 . Unimodal curves were also found for the simulations (Fig. 5) with a maximum between 0.01 and 0.1 s^{-1} , when combined with literature values for low shear blood viscosity,¹ these shear rates yield shear stress levels consistent with Chen *et al.*¹⁰ Other literature reports using different experimental methods have indicated similar results: (1) Aggregation measured using ultrasound analysis of porcine blood tube flow was maximum when the SR was between 0.1 and

1 s^{-1} ³⁰; (2) Copley *et al.*¹² employed an erythrocyte sedimentation rate method with human blood and found a maximum at about 0.1 s^{-1} (as indicated in Fig. 5).

Effects of Varying the Aggregation Force

It is well known that RBC aggregation in polymer solutions is influenced by polymer concentration and size.²⁹ Our theoretical approach was able to adequately describe the effects of these variables on MAS: increasing the concentration of macromolecules (i.e., changing the force intensity, see Fig. 6) or increasing the polymer molecular mass (i.e., altering the depletion layer thickness, see Fig. 7) both effected MAS. Note that increasing the concentration of macromolecules does not necessarily increase the aggregation force since the relationship between concentration and interaction energy is not linear.²⁹ Our results fully concur with data indicating that increasing the concentration up to a certain level, or increasing polymer molecular mass increases MAS for low SRs. *In vivo* studies in skeletal muscle venules are also consistent with our results: RBC aggregate size is larger than for native plasma when 500 kDa dextran is infused.⁵

Effects of Imposing Pulsatile SRs

It is well established that blood is non-Newtonian and can exhibit viscoelastic and thixotropic behaviors.^{7,8,18,32} According to Stoltz and Lucius,³²

reversible RBC aggregation is the major factor accounting for the viscoelastic and thixotropic behaviors of blood. Bureau *et al.*⁷ experimentally showed the complex behavior of blood using triangular steps of SRs; they obtained a hysteresis loop for the shear stress as a function of SR, which can be matched to the hysteresis in the MAS function for SR shown in Figs. 9 and 10. Recently, Owens²⁷ proposed a new constitutive blood model that takes into account aggregation and disaggregation of RBCs and that exhibits viscoelasticity and thixotropy. He simulated a shear rate-time profile reproduced in Fig. 9, thus allowing comparison of ours and his MAS results; as expected, a good agreement was found for the relationship between MAS and SR when a triangular step of SRs is applied to aggregated blood. Fitting Owen's data gave values of parameters $B = 10^7$ and $DA = 3 \times 10^{-26}$.

Model Limitations

Two-Dimensional Space

By definition in this paper, H was a surface ratio of RBCs within a ROI and not a volumetric ratio. Consequently, the simulated hematocrit does not precisely correspond to a true hematocrit of 40% of real blood. For given balance of attracting and repulsive forces considered here, the two-dimensional space imposed a limit on the possibility of particle interaction; therefore, for a three-dimensional volume, the parameters of our model would need to be adjusted.

RBC Properties

In our model, RBCs were designed as spheres instead of three-dimensional, biconcave and flexible objects. These characteristics promote the formation of rouleaux, which was not observed with our model.

Simple Couette Flow

Modeling Couette flow was a strategic selection because the constant shear rate characteristic simplified the selection of parameters allowing reproducing realistic RBC aggregation conditions. Future improvements of this model would be to adapt the flow of RBCs to realistic vessel geometries and to the RBC spatial arrangement. Indeed, RBC aggregation influences the local viscosity and consequently affects the velocity gradient. To achieve this goal in further improvements of our model, an Eulerian–Lagrangian approach can be explored. In the Lagrangian system, discrete particle trajectories are computed, whereas for a fluid model based on an Eulerian approach, the plasma phase is regarded as a continuum with balance of mass and momentum requiring writing of differential equations.

So, the solid phases (RBCs) describe in the present study would need to be coupled with the fluid phase by a relaxation time that is determined by the drag force due to slip velocity between phases. It would also be possible to correct for the local viscosity by taking into account the local density of RBCs. This strategy may allow to simulate changes in velocity profiles with increasing RBC aggregation, as expected from experimental results. To conclude, modeling of Couette flow was a necessary first step to manage the RBC aggregation as a function of the local flow condition (shear rate), aggregation force intensity and time.

CONCLUSION

A particle dynamic model was developed for RBC aggregation in shear flow. It was used to study the influence of SR, and aggregation force. This latter point is a very interesting specificity of this mechanical model. Indeed, it took into account a fragile balance between cell aggregation force and the dispersing effect of SR. The theoretical role of several parameters was identified: the intensity of aggregation force and SR in steady state MAS, and depletion layer thickness, on aggregation speed.

Also, it was illustrated that this mechanical model was capable of linking macroscopic blood properties (non-Newtonian and viscoelasticity) with micromechanical cell interactions. It would be very interesting to adapt the model for the complex study of aggregation in microcirculation flows, where these properties should be considered because of the importance of particle interactions. To what extent RBC aggregation in capillaries may affect global hemodynamics is not fully understood, as are the inherent mechanisms. Undeniably, a RBC model is still lacking to more thoroughly investigate the impact of different levels of aggregation, deformability and H on flows within complex geometries, such as bifurcations and junctions. Other effects resulting from the organization of particles could also be studied, such as the impact of RBC aggregates on axial leukocyte and platelet migration as well as their adhesion on the vascular endothelium.

ACKNOWLEDGMENTS

This work was supported by joint funding from the National Institutes of Health of the USA (#RO1HL 078655), the Canadian Institutes of Health Research (#CMI 72323) and the Heart and Stroke Foundation of Canada (#PG-05-0313). Dr. Guy Cloutier was the

recipient of a National Scientist Award from the “Fonds de la recherche en santé du Québec” (2004–2009). We are indebted to the “Réseau Québécois de Calcul de Haute performance” (RQCHP) for the generous allocation of computer resources. The authors thank Mr. Ovid Da Silva, Research Support Office, Research Center of the University of Montreal Hospital, CRCHUM, for editing this manuscript.

REFERENCES

- ¹Alexy, T., R. B. Wenby, E. Pais, L. J. Goldstein, W. Hogenauer, and H. J. Meiselman. An automated tube-type blood viscometer: validation studies. *Biorheology* 42:237–247, 2005.
- ²Armstrong, J. K., R. B. Wenby, H. J. Meiselman, and T. C. Fisher. The hydrodynamic radii of macromolecules and their effect on red blood cell aggregation. *Biophys. J.* 87:4259–4270, 2004. doi:10.1529/biophysj.104.047746.
- ³Bagchi, P. Mesoscale simulation of blood flow in small vessels. *Biophys. J.* 92:1858–1877, 2007. doi:10.1529/biophysj.106.095042.
- ⁴Baumler, H., E. Donath, A. Krabi, W. Knippel, A. Budde, and H. Kiesewetter. Electrophoresis of human red blood cells and platelets. Evidence for depletion of dextran. *Biorheology* 33:333–351, 1996. doi:10.1016/0006-355X(96)00026-1.
- ⁵Bishop, J. J., A. S. Popel, M. Intaglietta, and P. C. Johnson. Effect of aggregation and shear rate on the dispersion of red blood cells flowing in venules. *Am. J. Physiol. Heart Circ. Physiol.* 283:H1985–H1996, 2002.
- ⁶Boryczko, K., W. Dzwinel, and D. A. Yuen. Dynamical clustering of red blood cells in capillary vessels. *J. Mol. Model.* 9:16–33, 2003.
- ⁷Bureau, M., J. C. Healy, D. Bourgoin, and M. Joly. Etude expérimentale IN VITRO du comportement rhéologique du sang en régime transitoire à faible vitesse de cisaillement. *Rheol. Acta* 17:612–625, 1978.
- ⁸Bureau, M., J. C. Healy, D. Bourgoin, and M. Joly. Rheological hysteresis of blood at low shear rate. *Biorheology* 17:191–203, 1980.
- ⁹Chen, J. Y., and Z. Q. Huang. Analytical model for effects of shear rate on rouleau size and blood viscosity. *Biophys. Chem.* 58:273–279, 1996. doi:10.1016/0301-4622(95)00105-0.
- ¹⁰Chen, S. Q., G. Barshtein, B. Gavish, Y. Mahler, and S. Yedgar. Monitoring of red-blood-cell aggregability in a flow-chamber by computerized image-analysis. *Clin. Hemorheol.* 14:497–508, 1994.
- ¹¹Chien, S., and K. M. Jan. Ultrastructural basis of mechanism of rouleaux formation. *Microvasc. Res.* 5:155–166, 1973. doi:10.1016/0026-2862(73)90068-X.
- ¹²Copley, A. L., R. G. King, and C. R. Huang. Erythrocyte sedimentation of human-blood at varying shear rates. *Biorheology* 13:281–286, 1976.
- ¹³Drochon, A., D. Barthes-Biesel, C. Lacombe, and J. C. Lelievre. Determination of the red-blood-cell apparent membrane elastic-modulus from viscometric measurements. *J. Biomech. Eng. Trans. ASME* 112:241–249, 1990.
- ¹⁴Duran, J. Modélisations numériques. In: Sables, poudres et grains: introduction à la physique des milieux granulaires. P. Eyrolles Sciences, 1997, pp. 215–226.
- ¹⁵Dzwinel, W., K. Boryczko, and D. A. Yuen. A discrete-particle model of blood dynamics in capillary vessels. *J. Colloid Interface Sci.* 258:163–173, 2003. doi:10.1016/S0021-9797(02)00075-9.
- ¹⁶Fontaine, I., D. Savery, and G. Cloutier. Simulation of ultrasound backscattering by red cell aggregates: effect of shear rate and anisotropy. *Biophys. J.* 82:1696–1710, 2002. doi:10.1016/S0006-3495(02)75522-7.
- ¹⁷Helbing, D., I. Farkas, and T. Vicsek. Simulating dynamical features of escape panic. *Nature* 407:487–490, 2000. doi:10.1038/35035023.
- ¹⁸Huang, C. R., N. Siskovic, R. W. Robertson, W. Fabisiak, E. H. Smitherberg, and A. L. Copley. Quantitative characterization of thixotropy of whole human-blood. *Biorheology* 12:279–282, 1975.
- ¹⁹Lim, B., P. A. J. Bascom, and R. S. C. Cobbold. Simulation of red blood cell aggregation in shear flow. *Biorheology* 34:423–441, 1997. doi:10.1016/S0006-355X(98)00025-0.
- ²⁰Liu, Y. L., and W. K. Liu. Rheology of red blood cell aggregation by computer simulation. *J. Comput. Phys.* 220:139–154, 2006. doi:10.1016/j.jcp.2006.05.010.
- ²¹Liu, Y. L., L. Zhang, X. Wang, and W. K. Liu. Coupling of Navier–Stokes equations with protein molecular dynamics and its application to hemodynamics. *Int. J. Numer. Methods Fluids* 46:1237–1252, 2004. doi:10.1002/fld.798.
- ²²Neu, B., J. K. Armstrong, T. C. Fisher, and H. J. Meiselman. Aggregation of human RBC in binary dextran–PEG polymer mixtures. *Biorheology* 38:53–68, 2001.
- ²³Neu, B., and H. J. Meiselman. Sedimentation and electrophoretic mobility behavior of human red blood cells in various dextran solutions. *Langmuir* 17:7973–7975, 2001. doi:10.1021/la010945+.
- ²⁴Neu, B., and H. J. Meiselman. Depletion-mediated red blood cell aggregation in polymer solutions. *Biophys. J.* 83:2482–2490, 2002. doi:10.1016/S0006-3495(02)75259-4.
- ²⁵Neu, B., and H. J. Meiselman. Depletion interactions in polymer solutions promote red blood cell adhesion to albumin-coated surfaces. *Biochim. Biophys. Acta* 1760:1772–1779, 2006.
- ²⁶Noguchi, H., and G. Gompper. Shape transitions of fluid vesicles and red blood cells in capillary flows. *Proc. Natl Acad. Sci. USA* 102:14159–14164, 2005. doi:10.1073/pnas.0504243102.
- ²⁷Owens, R. G. A new microstructure-based constitutive model for human blood. *J. Non-Newton Fluid Mech.* 140:57–70, 2006.
- ²⁸Pivkin, I. V., P. D. Richardson, and G. Karniadakis. Blood flow velocity effects and role of activation delay time on growth and form of platelet thrombi. *Proc. Natl Acad. Sci. USA* 103:17164–17169, 2006. doi:10.1073/pnas.0608546103.
- ²⁹Rampling, M. W., H. J. Meiselman, B. Neu, and O. K. Baskurt. Influence of cell-specific factors on red blood cell aggregation. *Biorheology* 41:91–112, 2004.
- ³⁰Shehada, R. E. N., R. S. C. Cobbold, and L. Y. L. Mo. Aggregation effects in whole-blood—influence of time and shear rate measured using ultrasound. *Biorheology* 31:115–135, 1994.
- ³¹Stoltz, J. F., and M. Donner. Red blood cell aggregation: measurements and clinical applications. *Trans. J. Med. Sci.* 15:26–39, 1991.
- ³²Stoltz, J. F., and M. Lucius. Viscoelasticity and thixotropy of human-blood. *Biorheology* 18:453–473, 1981.

³³Sutera, S. P., P. R. Pierre, and G. I. Zahalak. Deduction of intrinsic mechanical-properties of the erythrocyte-membrane from observations of tank-treading in the rheoscope. *Biorheology* 26:177–197, 1989.

³⁴Zhang, J. F., P. C. Johnson, and A. S. Popel. Red blood cell aggregation and dissociation in shear flows simulated by lattice Boltzmann method. *J. Biomech.* 41:47–55, 2008. doi:[10.1016/j.jbiomech.2007.07.020](https://doi.org/10.1016/j.jbiomech.2007.07.020).